# A Fast Algebraic Estimator for System Parameter Estimation and Online Controller Tuning—A Nanopositioning Application

Andres San-Millan, Sumeet S. Aphale, *Senior Member, IEEE*, and Vicente Feliu, *Senior Member, IEEE*

***Abstract*—Parameter uncertainty is a key challenge in the real-time control of nanopositioners employed in scanning probe microscopy. Changes in the sample to be scanned introduces changes in system resonances, requiring instantaneous online tuning of controller parameters to ensure stable, optimal scanning performance. This paper presents a method based on the frequency-domain algebraic derivative approach for the accurate online identification of the nanopositioner's parameters. The parameter estimates are produced within a fraction of one period of the resonant mode frequency, allowing almost instantaneous tuning of controller parameters. Experimental results show that the proposed method can be utilized to automatically tune an integral resonant control scheme that combines both damping and tracking actions, and consequently deliver positioning performance far superior to that achieved solely due to the scheme's inherent robustness properties. It is further shown that the achieved performance compares favorably with an optimally designed control scheme of the same type.**

***Index Terms*—Algebraic parameter estimation, integral resonant control, nanopositioning.**

## I. Introduction

HIGH-SPEED nanopositioning is a key enabler in several scientific areas such as biotechnology [1], [2], fibre optics [3], medicine [4], sensing [5], etc. Piezoelectric-stack driven nanopositioners have gained high popularity in recent years [6], due to their numerous advantages such as mechanical robustness, relatively large travel ranges, high resolution, repeatability, accuracy, and absence of friction or stiction. The resonant dynamics of these nanopositioners, combined with the nonlinear effects induced by the piezoelectric actuators, i.e., hysteresis and creep, mandate the design and implementation of an effective closed-loop control scheme to achieve accurate positioning performance. Consequently, most popular control schemes incorporate both damping (for the mechanical resonances) and tracking (for accurate positioning) actions, [7].

During active scanning operations, changes in resonant frequency by up to 80% can be introduced by numerous factors. Some of these changes can be estimated to a certain extent—for example—changes in the mass of the sample scanned, additional mass introduced by heating elements, magnetic coils or liquid cells, etc. On the other hand, changes in the temperature, humidity, payload during pick and place tasks at nanometric scale, tribology variations, etc., are difficult to predict [8]. This uncertainty in key system parameters makes it extremely difficult to design effective controllers, as most control design techniques (and performance thereof) are based on an accurate system model [9]. Till date, this parameter uncertainty was addressed by ascertaining that the designed control scheme was robust to parameter variations within a certain operational limit. Consequently, several control techniques that possess adequate robustness have been proposed [10]–[15]. These techniques, though robust, undergo considerable degradation in positioning performance when the system moves away from the nominal model parameters on which the controller design was initially based. This is why many commercial nanopositioners define a limited range of admissible payloads (changes in mass results in subsequent changes in resonant frequency) and indicate the maximum scanning frequency associated with each mass, for which the nanopositioners deliver acceptable positioning performance.

To overcome this limitation, this paper applies the general algebraic framework for linear identification proposed in [16], to formulate a specific algorithm aimed at the online parameter estimation of a lightly damped second-order systems, hitherto not addressed in the literature. Furthermore, a new reinitiation algorithm is also proposed. Though several reinitiation algorithms have been published in the literature, arguably the more efficient one was reported in [17]. The reinitiation algorithm proposed in this paper outperforms the one presented in [17] by: 1) requiring less computational effort and computer memory and 2) ensuring smooth convergence to zero, thereby yielding parameter

Manuscript received January 16, 2018; revised May 13, 2018 and June 27, 2018; accepted July 24, 2018. Date of publication September 3, 2018; date of current version January 31, 2019. This work was supported in part by the Spanish Agencia Estatal de Investigacion under Project DPI2016-80547-R (Ministerio de Economia y Competitividad), in part by the European Social Fund (FEDER, EU), and in part by the Spanish FPU12/00984 Program (Ministerio de Educacion, Cultura y Deporte). *(Corresponding author: Andres San-Millan.)*

A. San-Millan and V. Feliu are with the Instituto de Investigaciones Energéticas y Aplicaciones Industriales, Escuela Técnica Superior de Ingenieros Industriales, Universidad de Castilla-La Mancha, 13071 Ciudad Real, Spain (e-mail: andres.sanmillan@uclm.es; vicente.feliu@uclm.es).

S. S. Aphale is with the Center for Applied Dynamics Research, School of Engineering, University of Aberdeen, Aberdeen AB24 3UE, U.K. (e-mail: s.aphale@abdn.ac.uk).

Color versions of one or more of the figures in this paper are available online at http://ieeexplore.ieee.org.

Digital Object Identifier 10.1109/TIE.2018.2863206

estimates in less time (typically shorter than one period of the resonance frequency). Moreover, previous works [18] and [19] identified only two parameters of slowly oscillating systems (the resonance frequencies were under 2 Hz). The algorithm proposed in this paper is capable of identifying three parameters of significantly fast oscillating system (resonance frequency >700 Hz) in less than one period of the resonance frequency, using relatively low sampling rates and limited computation capabilities. The proposed estimator is especially well-suited to track step-wise changes in system parameters such as those introduced by the addition or removal of mass (effected by changes in the scanned sample) on the nanopositioner. These estimates can further be utilized to automatically tune a multitude of popular control schemes applied to nanopositioners. Due to its simplicity, inherent robustness, good performance, and guaranteed stability, the integral resonant control (IRC) scheme that combines both damping and tracking actions [12] has been chosen as a candidate to demonstrate the efficacy of the proposed algebraic estimation and reinitiation algorithm.

This paper is organized as follows. Section II formally states the problem and presents the algebraic estimation scheme utilized in this work. The experimental setup is described in Section III. Simulated as well as real-time experimental results that validate the proposed algebraic estimator are presented and discussed in Section IV. Section V concludes the paper.

## II. Problem Statement and Background Theory

The frequency-response of one axis of a typical nanopositioner exhibits a dominant lowly damped resonant peak and can be modeled with good accuracy, as a lightly damped mass-spring-damper system whose dynamics can be described by

$$\ddot{y}(t) + 2\zeta\omega_n \dot{y}(t) + \omega_n^2 y(t) = \sigma^2 u(t) \tag{1}$$

where $y(t)$ is the displacement of the moving platform, $u(t)$ is the input voltage applied to the actuator, $\sigma^2$ corresponds to the equivalent stiffness of the mechanism, $\zeta$ is the damping coefficient, and $\omega_n$ is the natural frequency of vibration of the system [20]. To initiate any control design, the system parameters $\sigma$, $\zeta$, and $\omega_n$ need to be estimated accurately from $u(t)$ and $y(t)$. These system parameters are often time-variant. Furthermore, these estimated parameters are often utilized to tune a controller in an adaptive control scheme. Thus, the desirable features for an appropriate estimation algorithm are as follows.

1) *Short Estimation Time:* The time required to generate an accurate estimate must be shorter than one period of the targeted resonant mode frequency. This will enable quick tuning of the controller parameters without long periods of subpar performance due to an incorrectly tuned controller. Since the nanopositioner used in the experiments to verify this work exhibits its first resonant mode at ≈700 Hz, an estimation time of the order of 1 ms is required.
2) *Robustness to Unmodeled Dynamics:* The system is modeled as a second-order resonant system, yet, as seen in Section III, at least four high-frequency resonant modes can be seen in the recorded frequency response for the nanopositioner axis. As the frequency of the second mode is less than two times the frequency of the first mode, it is apparent that the second mode will have a clear impact on the output signal and can potentially introduce errors in any system parameters identified based on a single resonant-mode model.
3) *Practicality and Applicability:* The algorithm should be implementable on a standard PC with modest computation capabilities and be relatively insensitive to coarse sampling. Furthermore, the identification algorithm must be relatively simple in order to facilitate real-time implementation. For the system used to conduct experiments reported in Section III, the sampling rate is about 30 $\mathrm{KSs}^{-1}$. Therefore, each period of the first resonant mode is characterized by only 30–40 samples (and a significantly less number of samples characterize the higher modes).

Phase-locked-loop topologies [21], adaptive notch filters [22], robust globally convergent estimators [23], continuous least squares [24], frequency-locked-loop filters [25], and Prony-based methods [26] have all been applied to estimate the parameters of undamped resonant modes. However, these methods show high sensitivity to noise as well as the neglected high-frequency modes and, in most instances, are incapable of providing good estimates for systems with lightly damped resonant modes, typical of nanopositioner axes. Additionally, these methods require time equivalent to several periods of the resonant frequency to generate an accurate estimate of the system parameters. All these drawbacks are overcome by algebraic estimators [27], [28]. Continuous transfer functions have also been obtained using algebraic identification techniques, having mainly been applied to electrical drives [29], [30]. It was shown in [31] that algebraic identification methods converge to accurate estimates in significantly less time compared to algorithms based on discrete least squares. Moreover, algebraic identification techniques are based on relatively simple algorithms that can be easily implemented in real time, and possess low sensitivity to slow sampling rates.

As the algebraic identification technique possesses all the desirable features listed earlier, it emerges as the most appropriate approach to be applied to parameter identification and controller tuning for nanopositioning applications.

### A. Estimation Algorithm

The Laplace transform of the equation of motion of a single mass-spring-damper system presented in (1) is given by

$$\sigma^2 U(s) = s^2 Y(s) - sy(0) - \dot{y}(0) + 2\zeta\omega_n \left[sY(s) - y(0)\right] + \omega_n^2 Y(s) \tag{2}$$

where $Y$ and $U$ are the Laplace transforms of $y(t)$ and $u(t)$, respectively. Double differentiation with respect to the complex variable "s" cancels the initial conditions

$$\frac{\partial^2 U}{\partial s^2} = \frac{1}{\sigma^2}\left[2Y + 4s\frac{\partial Y}{\partial s} + s^2\frac{\partial^2 Y}{\partial s^2}\right] + \frac{2\zeta\omega_n}{\sigma^2}\left[2\frac{\partial Y}{\partial s} + s\frac{\partial^2 Y}{\partial s^2}\right] + \frac{\omega_n^2}{\sigma^2}\frac{\partial^2 Y}{\partial s^2}. \tag{3}$$

In order to avoid multiplications by positive powers of $s$, which are translated as undesirable time derivatives in the time-domain, we multiply (3) by $s^{-2}$. Rearranging this expression, we obtain

$$s^{-2}\frac{\partial^2 U}{\partial s} = \frac{1}{\sigma^2}\left[2Ys^{-2} + 4s^{-1}\frac{\partial Y}{\partial s} + \frac{\partial^2 Y}{\partial s^2}\right] + \frac{2\zeta\omega_n}{\sigma^2}\left[2s^{-2}\frac{\partial Y}{\partial s} + s^{-1}\frac{\partial^2 Y}{\partial s^2}\right] + s^{-2}\frac{\omega_n^2}{\sigma^2}\frac{\partial^2 Y}{\partial s^2}. \quad (4)$$

Let $\mathcal{L}$ denote the usual operational calculus transform acting on exponentially bounded signals with bounded left support [32]. Recall that $\mathcal{L}^{-1}s(\cdot) = d/dt(\cdot)$, $\mathcal{L}^{-1}1/s(\cdot) = \int_0^t(\cdot)(\sigma)d\sigma$, and $\mathcal{L}^{-1}d^v/ds^v(\cdot) = (-1)^v t^v(\cdot)$. Expression (4) can thus be written in the time domain as follows:

$$\int^2 t^2 u = \frac{1}{\sigma^2}\left[2\int^2 y - 4\int ty + t^2 y\right] + \frac{2\zeta\omega_n}{\sigma^2}\left[-2\int^2 ty + \int t^2 y\right] + \frac{\omega_n^2}{\sigma^2}\int^2 t^2 y. \quad (5)$$

Expression (5) can be written in a compact form as

$$q(t) = \frac{1}{\sigma^2}\beta(t) + \frac{2\zeta\omega_n}{\sigma^2}\xi(t) + \frac{\omega_n^2}{\sigma^2}\eta(t) \quad (6)$$

where $q(t)$, $\beta(t)$, $\xi(t)$, and $\eta(t)$ can be calculated in real time as they are the outputs of the following time-varying linear unstable filters

$$\begin{array}{llll} q(t) = z_1 & \beta = z_3 + t^2 y & \xi = z_5 & \eta = z_7 \\ \dot{z_1} = z_2 & \dot{z_3} = z_4 - 4ty & \dot{z_5} = z_6 + t^2 y & \dot{z_7} = z_8 \\ \dot{z_2} = t^2 u & \dot{z_4} = 2y & \dot{z_6} = -2ty & \dot{z_8} = t^2 y \end{array} \quad (7)$$

whose initial states are set to zero.

The linear equation (6) has three unknowns, $\sigma$, $\zeta$ and $\omega_n$, which can be obtained from a least-squares error fitting in the time interval $[t_i, t_f]$ (where the interval $[t_i, t_f]$ is equal to the interval of time between the first and the last available sample). With a change of variables such that

$$A = \frac{1}{\sigma^2}, B = \frac{2\zeta\omega_n}{\sigma^2}, C = \frac{\omega_n^2}{\sigma^2} \quad (8)$$

a cost function can be defined as

$$\varepsilon = \int_{t_i}^{t_f}\left\{\left[\beta(\tau)\ \xi(\tau)\ \eta(\tau)\right]\cdot\begin{bmatrix}A\\B\\C\end{bmatrix} - q(\tau)\right\}^2 d\tau. \quad (9)$$

The minimization of this cost function leads to

$$\begin{bmatrix}A\\B\\C\end{bmatrix} = \left[\int_{t_i}^{t_f}\begin{bmatrix}\beta(\tau)\\\xi(\tau)\\\eta(\tau)\end{bmatrix}\cdot\left[\beta(\tau)\quad\xi(\tau)\quad\eta(\tau)\right]d\tau\right]^{-1} \cdot\int_{t_i}^{t_f}\begin{bmatrix}\beta(\tau)\\\xi(\tau)\\\eta(\tau)\end{bmatrix}q(\tau)d\tau. \quad (10)$$

The batch formula expressed in (10) was first applied for algebraic parameter estimation in [29]. Furthermore, a recursive formula of the least-squares algorithm that demonstrated increased computational efficiency was used in [30] to estimate the parameters of a dc motor using an algebraic estimator. The parameters $\sigma$, $\zeta$, and $\omega_n$ are only weakly linearly identifiable. This signifies that once $A$, $B$, and $C$ have been identified, $\sigma$, $\zeta$, and $\omega_n$ can be easily determined by using the following nonlinear relations:

$$\sigma = \frac{1}{\sqrt{A}}, \qquad \zeta = B\sqrt{\frac{1}{4AC}}, \qquad \text{and} \qquad \omega_n = \sqrt{\frac{C}{A}}. \quad (11)$$

### B. Reinitiation Algorithm

In order to perform the online estimation of the nanopositioner parameters, it is necessary to reset and reinitiate the aforementioned algorithm because: 1) linear time-varying filters are unstable, and the values of the variables involved in the estimation may therefore become very large as time increases and 2) the noise present in the measurements may produce wrong estimates such as negative values for $\sigma$, $\zeta$, and $\omega_n$. To avoid these issues, it is important to have a criterion, which clearly discriminates between two cases: 1) the estimator is providing good estimates and the procedure has converged to meaningful close-to-actual estimates of the parameters and 2) the samples utilized to produce the estimates cannot converge and it is necessary to reinitiate the estimation algorithm.

In order to determine the time of reinitiation, Pereira *et al.* [17] proposed a criterion based on the moving average and on the moving standard deviation of the estimates of frequency. However, these operations require the storage of a relatively high number of samples that comprise the moving window that is utilized to perform the average and the standard deviation. It is important to note that even if the recursive implementation of these operations is performed, all the samples need to be stored in a circular array. This may cause issues if the system presents limited memory or if it takes a long time to displace all the samples through the circular array.

To overcome the aforementioned issues and to utilize a more computationally efficient approach, the proposed procedure is based on the exponentially weighted moving average (EWMA) and the exponentially weighted moving standard deviation (EWMSTD) [33]. These two operators are commonly employed in forecasting seasonals and trends in economics. However, to the best of the authors' knowledge, this is the first time this criterion is used to define the reinitiation procedure of an algebraic estimator. The recursive formulae of the EWMA and the EWMSTD are given below

$$Z(i) = \lambda_1 \cdot X(i) + (1-\lambda_1)Z(i-1) \quad (12)$$

and

$$S(i) = \sqrt{\lambda_2(X(i) - Z(i))^2 + (1-\lambda_2)S^2(i-1)} \quad (13)$$

where $Z(i)$ is the EWMA computed for the $i$th sample $X(i)$, $S(i)$ is the $i$th EWMSTD computed for the $i$th sample $X(i)$, and $\lambda_j$, $0 < \lambda_j \leq 1$, $j = 1, 2$ are two smoothing constants. In

both cases, the initialization values are defined as $Z(1) = X(1)$ and $S(1) = X(1)$. It is important to note that from a control point of view, the EWMA is just a different representation of the discrete euler backward implementation of a first-order low-pass filter. By using these definitions and the outputs of the algebraic estimator provided by (11), it can be concluded that the estimation has converged when the following condition:

$$\frac{S_{\omega_n}(n)}{|Z_{\omega_n}(n)|} \leq \delta \quad \cap \quad Z_\sigma(n) > 0 \quad \cap \quad Z_\zeta(n) > 0 \qquad (14)$$

is verified. $S_{\omega_n}(n)$ and $Z_{\omega_n}(n)$ are the standard deviation and the average value of the estimated natural frequency of the system computed by using the EWMA and the EWMSTD. $\delta$ is the tolerance parameter that determines the accuracy of the estimate of the natural frequency of the system. Additionally, conditions $Z_\sigma(n) > 0$ and $Z_\zeta(n) > 0$ are imposed to ensure $\sigma > 0$ and $\zeta > 0$. Considering $T_s$ to be the sampling time, the sample under which condition (14) is verified is denoted as $\hat{n}$, and the time $\hat{n} \cdot T_s$ is the operation time interval corresponding to the interval of time from the beginning of the estimation process (it is assumed that $n = 0$ when the estimation starts) until (14) is satisfied. The estimates provided by the algorithm are

$$\omega_n^e = Z_{\omega_n}(\hat{n}), \qquad \sigma^e = Z_\sigma(\hat{n}), \qquad \zeta^e = Z_\zeta(\hat{n}). \qquad (15)$$

If condition (14) is not verified after time $T_r$, the resulting estimates are deemed invalid and the algorithm is reinitiated. The selection of $T_r$ is based on experience: a good compromise is often that of choosing a value of the order of the period of the lowest frequency that has to be estimated.

The proposed real-time estimation algorithm can be summarized as follows.

1) Initiate the algorithm.
2) During each sampling period, use inputs of the Brunovsky filter (7), i.e., the voltage applied to the system $u$, the displacement of the nanopositioner $y$, and the time $t$ as input to the estimator and compute new estimates of system parameters ($\omega_n$, $\sigma$, and $\zeta$) using (10) and (11).
3) Compute (12) and (13) using successive estimates of $\omega_n$ $\sigma$, and $\zeta$.
4) Check the reinitiation criterion (14). If this criterion is verified, the last value of each EWMA will be considered a valid estimation of the system parameters (15). If a time $T_r$ is reached and (14) is not fulfilled, return to step 1).

In the next section, a brief description of the experimental setup employed to validate the efficacy of the proposed algorithm is presented, followed by both simulation and experimental results.

## III. Experimental Setup

The experimental setup pictured in Fig. 1, consists of a flexure-based $XY$ serial-kinematic nanopositioner, voltage amplifiers and displacement sensors. The nanopositioner is driven by two piezoelectric-stacks, each with a stroke of $\pm 20$ $\mu$m. The nanopositioner delivers translational motions along $x$- and $y$-axes, which are measured by a Microsense 4810 capacitive

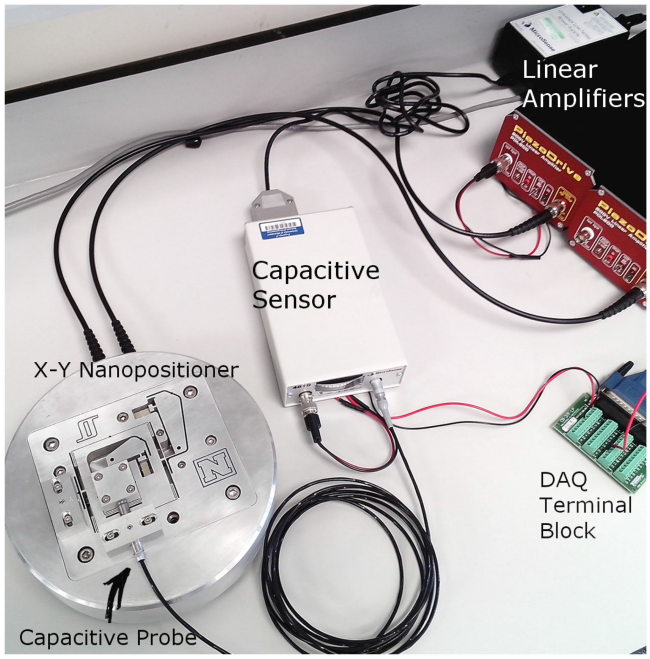


Fig. 1. Two-axis serial kinematic nanopositioner, designed at the EasyLab, University of Nevada, Reno.

displacement sensor and a 2805 measurement probe with a measurement range of $\pm 50$ $\mu$m for a corresponding voltage output of $\pm 10$ V. All experimental data are recorded in real time, using a PC OPTIPLEX 780 with an Intel Core2 Duo Processor running at 3.167 GHz and equipped with 2 GB of DDR3 RAM memory. The whole system is capable of deterministic sampling times as low as 30 $\mu$s. In order to interface between the nanopositioner and the PC, a PCI-6621 data acquisition card from National Instruments installed on a second PC running the real-time module from LabVIEW is utilized.

In order to characterize the dynamics of the nanopositioner, small signal frequency response functions (FRFs) were recorded. The FRFs are obtained by applying a sinusoidal chirp signal (from 10 to 1800 Hz) with an amplitude of 0.2 V as input to the voltage amplifier of the $x$-axis and measuring the output signal (sensor voltage proportional to axial displacement) along the same axis. Subsequently, the FRF is computed by taking the Fourier transform of the recorded data. The same procedure was repeated for obtaining the $y$-axis FRF. It is important to note that since the capacitive sensor measures relative displacements from a zero point, before each experiment a new zero point is measured in order to avoid any offset in the measurements. In Fig. 2, the magnitude responses of the two axes of the nanopositioner are plotted (recorded using a sampling time of 50 $\mu$s).

The chosen frequency range captures the dominant resonant mode of the nanopositioner as well as a number of high-frequency secondary modes that can be neglected due to their low dynamic range when compared to the first dominant resonant mode. The identified transfer function parameters for both axes of the nanopositioner are given in Table I.

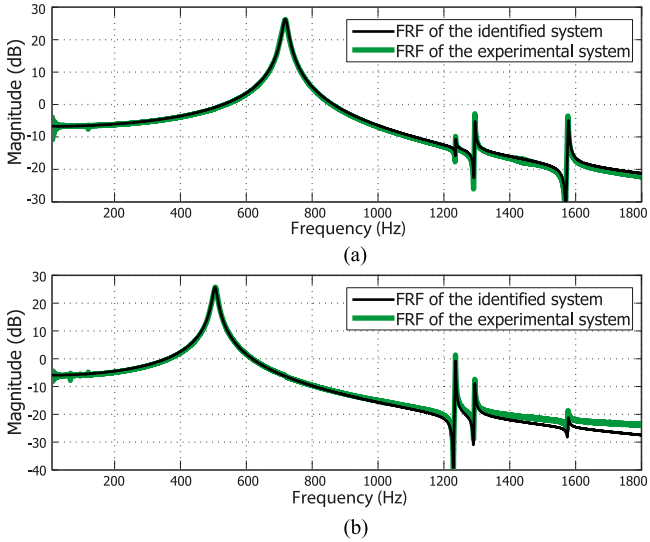


Fig. 2. (a) FRF of the $x$-axis and (b) FRF of the $y$-axis of the experimental platform.

TABLE I
PARAMETERS OF THE NANOPOSITIONER

| X axis | | | |
|---|---|---|---|
| Mode | Gain | Damping | Frequency (rad/s) |
| $1^{st}$ | $\sigma_1 = 3200$ | $\zeta_1 = 0.011$ | $\omega_1 = 716.2 \cdot 2\pi$ |
| $2^{nd}$ | $\sigma_2 = 250$ | $\zeta_2 = 0.0008$ | $\omega_2 = 1294 \cdot 2\pi$ |
| $3^{rd}$ | $\sigma_3 = 350$ | $\zeta_3 = 0.0008$ | $\omega_3 = 1578 \cdot 2\pi$ |
| $4^{th}$ | $\sigma_4 = 800$ | $\zeta_4 = 0.0001$ | $\omega_4 = 2325 \cdot 2\pi$ |
| Y axis | | | |
| Mode | Gain | Damping | Frequency (rad/s) |
| $1^{st}$ | $\sigma_1 = 2250$ | $\zeta_1 = 0.013$ | $\omega_1 = 505 \cdot 2\pi$ |
| $2^{nd}$ | $\sigma_2 = 250$ | $\zeta_2 = 0.0005$ | $\omega_2 = 1235 \cdot 2\pi$ |
| $3^{rd}$ | $\sigma_3 = 100$ | $\zeta_3 = 0.0008$ | $\omega_3 = 1578 \cdot 2\pi$ |
| $4^{th}$ | $\sigma_4 = 400$ | $\zeta_4 = 0.0001$ | $\omega_4 = 2325 \cdot 2\pi$ |

It is also important to note that the parameters of the system used in (1) correspond to the dominant first resonant mode of the corresponding axis as reported in Table I.

## IV. Real-Time Parameter Estimation of a Nanopositioner

The proposed algebraic estimator involves two algorithms: the estimation procedure and the convergence criterion. In Section IV-A, simulations are carried out to illustrate the accuracy, small convergence time of the estimator, and the effectiveness of the convergence criterion given by (14). Consequently, the experimental setup is utilized to validate the efficacy of the proposed technique using a practical application in Section IV-B. Results provided by the algebraic estimator are used to automatically tune the parameters of the IRC applied to impart damping to the first resonant mode of the nanopositioner axis (inner loop) as well as the integral controller gain (outer loop) that enforces reference tracking [12]. It is experimentally demonstrated that the proposed method is capable of tracking

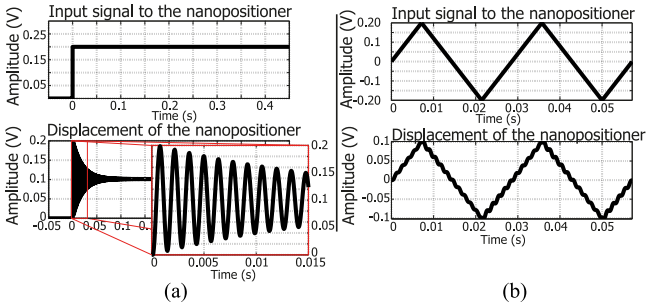


Fig. 3. Input signals applied to the simulated model of the nanopositioner and displacement produced.

step-wise changes in the parameters of the system and provides real-time estimations, which can be used to perform online automatic tuning of classical control schemes typically employed in nanopositioning systems, thus improving their performance.

### A. Simulated Results

The most popular trajectory nanopositioners are forced to follow is a raster pattern. This is generated by moving one axis of the nanopositioner in a triangular trajectory and the other in a stair-case trajectory. First, the identified model of the nanopositioner is utilized to simulate the response of the system to the two inputs: step and triangular signals. Later, using the the open-loop response of the system, the performance of the algebraic estimator in correctly estimating the parameters of the system is studied. To highlight the contribution of this paper and the advantages of the application of algebraic parameter estimation to a practical system, the relationship between the maximum achievable bandwidth (considering the $\pm 3$ dB criterion) and the variation in the resonant frequency of the nanopositioner axis are studied under two operating scenarios: 1) Nominal operation—The IRC-based control scheme is pretuned to the parameters of the unloaded nanopositioner and 2) Online algebraic estimation and tuning: The IRC-based control scheme is tuned online using the system parameter estimates obtained via the adopted algebraic estimation technique.

***1) Response to Triangular and Step Signals:*** Both the step and the triangular inputs have an amplitude of 0.2 V. The triangular input trajectory used to simulate the response of the system has a frequency of 35 Hz, see Fig. 3. The step response clearly shows high-frequency oscillations caused by the excitation of the first resonant mode of the system. These oscillations are utilized by the algebraic estimator to identify the parameters of the nanopositioner and, since the step signal produces oscillations with a higher amplitude than those produced by the triangular signal,[1] the step signal leads to estimates quicker than the triangular signal.

In order to illustrate the working principle of the proposed method and demonstrate its fast convergence capabilities, Fig. 4

[1]This is because the amplitude of the harmonic frequency component that excites the system resonance is higher in the step signal than in the triangular signal.

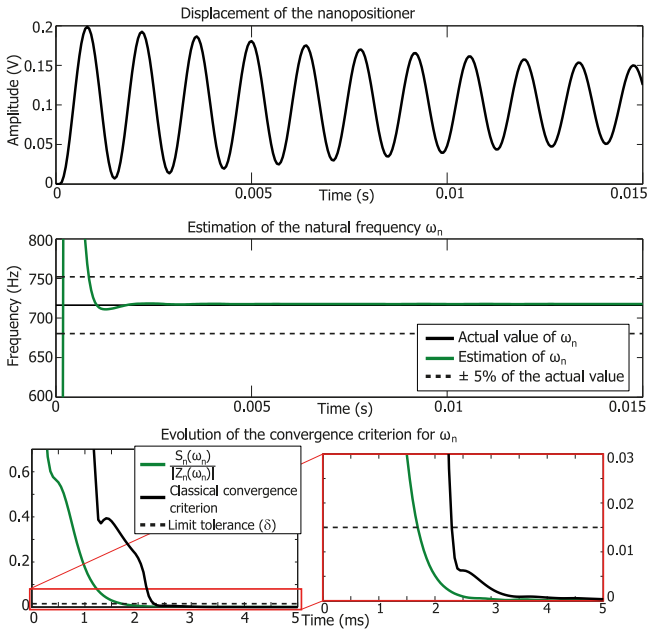


Fig. 4. Displacement of the simulated model of the nanopositioner when excited with a step signal. Evolution of the estimation of the natural frequency of the system over time, and evolution of the stop criterion.

shows the displacement of the nanopositioner when excited by the aforementioned step signal. The evolution of the estimation of the natural frequency of the system and a comparison between the evolution of the reinitiation condition $S_n(\omega_n)/|Z_n(\omega_n)|$ and the reinitiation condition proposed in [17] (possibly the most efficient of the conditions proposed in literature for algebraic estimators) are also presented. It is clear that the estimation of $\omega_n$ converges very quickly to its actual value, and that the convergence criterion is a monotonically decreasing function which tends to zero (a feature not achieved with the condition proposed in [17]). Note that the limit tolerance $\delta$ is reached in a very short time, and thus the condition (14) is verified. Consequently, the estimate of the natural frequency is produced in less than one cycle of the high-frequency oscillations experienced by the system. The evolution of the estimator in the case of a triangular signal is omitted because it presents a similar behavior but with slightly slower convergence.

Once the efficacy of the algebraic estimator and the convergence criterion are verified, the complete procedure (including the reinitiation step) is analyzed. In this case, the maximum time required to produce a valid estimation $T_r$ is set to 0.015 s. The resulting estimates can be seen in Fig. 5. Table II gives a comparison of the estimates produced by the algorithm for both step and triangular inputs.

Because the exact values of the parameters $\omega_n$, $\sigma$, and $\zeta$ are known in the simulation, the performance of the estimates is expressed in terms of relative error with regards to the actual values of the parameters of the system. As several estimates have been produced in each experiment (because every time the estimator is re-initiated, a new estimate is produced), the minimum, maximum, and average errors are shown along with the standard deviation of the errors of the estimation of each parameter.

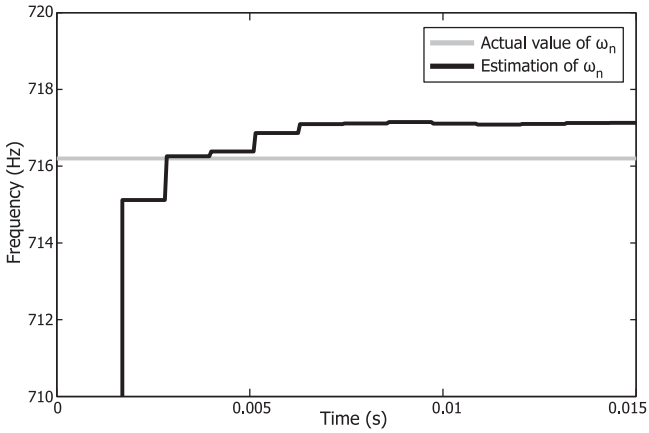


Fig. 5. Estimation of the natural frequency of the system excited by a step input signal.

TABLE II
QUANTIFYING ESTIMATOR PERFORMANCE

| Parameter | Min. Value | Average Value | Max. Value | Standard deviation |
|---|---|---|---|---|
| $\omega_n$ | 0.02 (%) | 0.11 (%) | 0.24 (%) | 0.028 (%) |
| $\sigma$ | 0.067 (%) | 0.23 (%) | 0.43 (%) | 0.052 (%) |
| $\zeta$ | 2.01 (%) | 14.76 (%) | 17.67 (%) | 3.28 (%) |
| Operation time interval (s) | 0.00105 | 0.00106 | 0.00165 | $8.24{\cdot}10^{-5}$ |
| Triangular input | | | | |
| Parameter | Min. Value | Average Value | Max. Value | Standard deviation |
| $\omega_n$ | 0.03(%) | 0.62 (%) | 2.30 (%) | 0.63 (%) |
| $\sigma$ | 0.02 (%) | 0.75 (%) | 2.66 (%) | 0.74 (%) |
| $\zeta$ | 16.35 (%) | 17.79 (%) | 18.53 (%) | 0.59 (%) |
| Operation time interval (s) | 0.00105 | 0.00109 | 0.0033 | 0.00031 |

The last index, which is utilized to describe the performance of the estimator, is the time required to generate each estimate. In each case, the maximum value corresponds to the time taken to produce the first estimate in each case. The time taken for the succeeding estimates is considerably shorter. Additionally, it can be seen that estimates derived with triangular input excitation constitute a larger error compared to those generated via step excitation. This is because of the smaller magnitude of high-frequency oscillations produced by the triangular signal. However, in both cases, the estimates of $\omega_n$ and $\sigma$ (which are the most important parameters required for the correct tuning of any control scheme) present an estimation error less than 3%.

***2) Performance Quantification in Closed-Loop:*** To demonstrate the efficacy and performance improvement facilitated by the proposed algebraic estimation with online tuning of control parameters, the proposed technique was compared with the traditional closed-loop approach where the controller parameters are pretuned for the nominal unloaded case. For both the traditional pretuned and the proposed online-tuned cases, the resonant mode frequency of the nanopositioner axis was reduced to simulate loading and the standard $\pm 3$ dB criterion was used a performance metric. In both cases, the control scheme used was an inner-loop integral resonant controller for damping and an outer-loop integral controller for tracking. Note

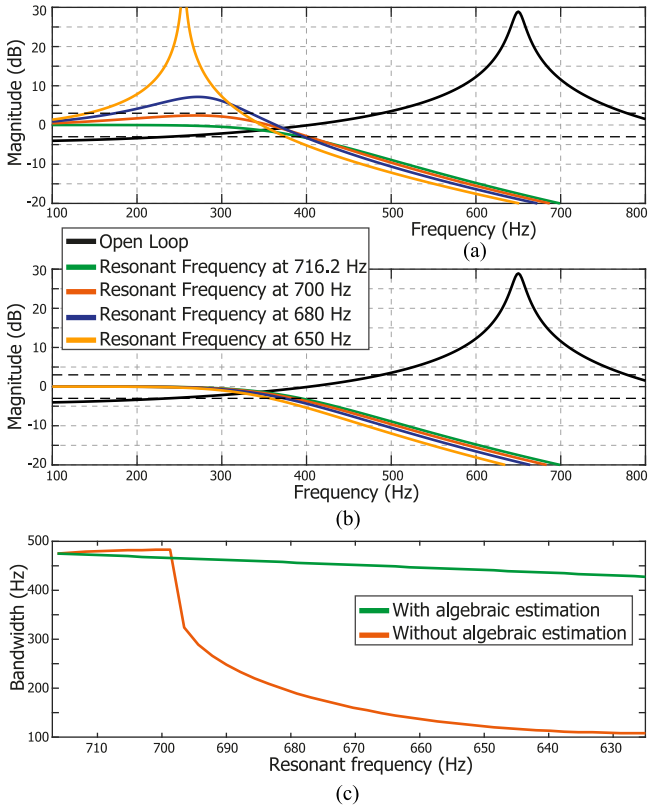


Fig. 6. Open- and closed-loop FRFs of a nanopositioner axis incorporating an IRC scheme with integral tracking designed using the (a) traditional pretuned approach, (b) proposed algebraic estimation with online tuning of controller parameters, and (c) relationship between closed-loop bandwidth and resonant frequency of the system for the traditional and proposed approaches.

that for the traditional pretuned case, closed-loop performance in the presence of variation in system parameters (resonance frequency and damping coefficient in this case) is solely dependent on the inherent robustness properties of the adopted control scheme. The simulation results are shown in Fig. 6.

As seen in Fig. 6(a), for the traditional pretuned case, the shape of the closed-loop FRF and therefore the resulting 3 dB bandwidth varies substantially and degrades rapidly as the resonant frequency moves away from the nominal unloaded case. The deterioration in the closed-loop bandwidth is clearly seen in Fig. 6(c). On the other hand, as the proposed scheme first estimates the system parameters (resonance frequency and the damping coefficient $\omega_n$ and $\zeta$) and then tunes the controller gains for every resonance frequency shift individually, the loss of bandwidth is more graceful and gradual when compared with the traditional pretuned case. This is evident from the FRF's presented in Fig. 6(b) as well as from the bandwidth versus resonance frequency plot given in Fig. 6(c).

## B. Experimental Results

As gleaned from the simulations, the worst case scenario for the algebraic estimator is the utilization of a triangular input signal, as it produces parameter estimates with larger average errors and requires a longer time to produce them. Therefore, to

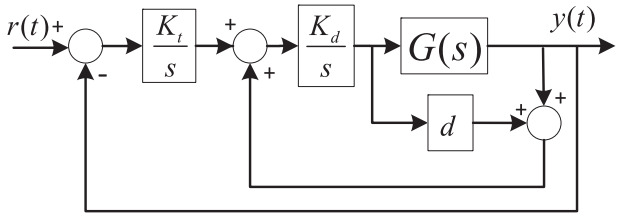


Fig. 7. Block diagram of the IRC control scheme combining both damping and tracking actions.

rigorously interrogate the effectiveness of the proposed scheme and demonstrate its potential for practical application, the worst case, i.e., employing a triangular signal for procuring parameter estimates, was chosen. It is obvious that the step signal input will result in more accurate estimates and improved estimator performance.

In this section, the estimates produced by the algebraic estimator are utilized to tune the parameters of the IRC-based damping combined with integral tracking, see Fig. 7. The three controller parameters that require tuning are: 1) the tracking gain - $K_t$, 2) the damping gain - $K_d$, and 3) the feed-through term - $d$. The appropriate values of these parameters are computed online using formulas provided in [34] viz:

$$\alpha = \sqrt{2^{3/2}+4}, \qquad \beta = \sqrt{2}+2$$

$$\omega_d = \frac{\omega_n \alpha \zeta + \omega_n \sqrt{(\alpha^2 - 4\beta)\zeta^2 + \beta}}{\beta}$$

$$K_d = \frac{-2\alpha\zeta\omega_d^3 + \omega_n \beta \omega_d^2 - \omega_n^3}{2\zeta\sigma^2}$$

$$d = \frac{\beta\sigma^2\omega_d^2 - \omega_n^2\sigma^2}{2\omega_n\alpha\zeta\omega_d^3 - \omega_n^2\beta\omega_d^2 + \omega_n^4}$$

$$K_t = \frac{2\zeta\omega_d^4}{\omega_n\beta\omega_d^2 - 2\alpha\zeta\omega_d^3 - \omega_n^3}. \tag{16}$$

These equations aim to place the closed-loop poles of the controlled system in a low-pass Butterworth pattern whose cutoff frequency corresponds to $\omega_d$. It can be seen that the design of the three parameters of the controller depends on the numerical values of the first resonant mode frequency $\omega_n$, the damping coefficient $\zeta$, and the dc gain factor $\sigma$. As these design rules place the closed-loop poles of the system in very definite positions, any change in the parameters of the nanopositioner would lead to a displacement of the closed-loop poles of the system and thus a degradation of the system's performance, which in extreme cases may lead to instability.

To demonstrate the effectiveness of the proposed algorithm, two scenarios are tested experimentally. In Case 1, assuming no previous knowledge of the system, the estimator first generates parameter estimates using the output of the nanopositioner axis under triangular wave excitation and then uses these estimates to tune the parameters of the IRC control scheme. In Case 2, the nanopositioner is assumed to be operating under nominal conditions and a sudden change in system parameters is introduced via loading. The proposed algorithm is tasked with

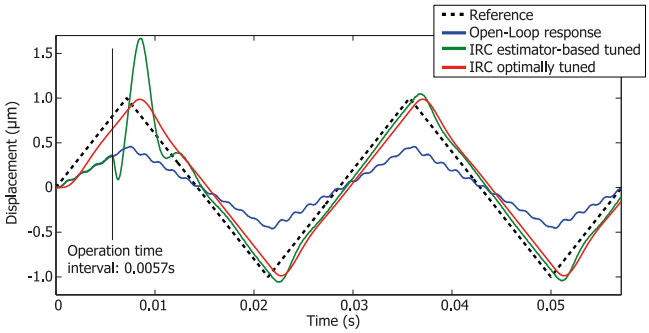


Fig. 8. Evolution of the estimates of the resonance frequency when the experimental system is excited with a triangular signal of 35 Hz. The time at which the algebraic estimator converges is indicated in the figure.

re-estimating the new system parameters and consequently tuning the control scheme parameters appropriately. To ensue that the proposed scheme works under all possible scenarios of parameter changes, Case 2 is further split into two subcases: 1) payload is increased and 2) payload is decreased.

***1) Case1—Parameter Estimation and Control Scheme Tuning Without Prior System Knowledge:*** In this experiment, the $X$-axis of the nanopositioner is excited in open loop with a triangular signal. The algebraic estimator is initialized to estimate the parameters of the system and the obtained estimates are given as inputs to the design rules of the IRC-based control scheme (16) (it is important to note that all this is done on-line and autonomously). Finally, once the parameters of the control scheme have been computed, the control scheme is applied to the system to enforce low-error reference tracking. For comparison, the experimental results obtained with this procedure and the experimental results obtained when the control scheme is designed knowing the identified parameters of the system (pretuned IRC scheme) are presented in Fig. 8. The open-loop response of the system and the time needed to produce the parameter estimates are also included.

It was noticed that when the reinitiation was triggered in this experiment after the first estimation, the design of the regulator was so effective that the displacement produced by the closed-loop system presents very small oscillations due to the dominant resonant mode. Thus, the estimator was unable to produce any further estimate (it was not able to fulfill (14) in a time $T_r = 0.015$ s).

***2) Case 2—Online tuning of the IRC Scheme When Payload is Increased (Resonance Frequency Decreases):*** This experiment was carried out as follows: The parameters of the $X$-axis of the nanopositioner were used to design the IRC-based control scheme by using (16). The resulting control scheme was then applied to the $Y$-axis and a 35 Hz triangular signal was used as the reference input. As seen from Table I and Fig. 2, the $Y$-axis has a much lower resonance frequency (505 Hz) compared to the $X$-axis (716 Hz) and therefore, this procedure effectively mimics a real-life scenario where a payload is added to the nanopositioner. Subsequently, the algebraic estimator was triggered to estimate the parameters of the $Y$-axis and retune the parameters of the control scheme in order to improve its performance.

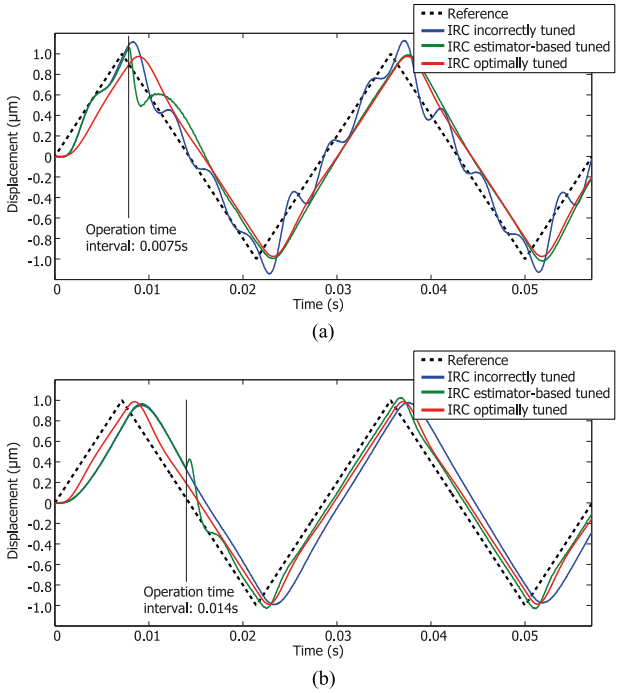


Fig. 9. Displacement of the nanopositioner before and after the estimation procedure in the case of (a) Increase in payload (decrease in resonance frequency) and (b) Decrease in payload (increase in resonance frequency). The operation time when the algebraic estimator has converged is clearly indicated.

The experimental results obtained with the nominal, pretuned IRC for the higher resonance frequency, the IRC designed using the proposed online-tuning scheme, and the IRC pretuned for the correct (reduced) resonance frequency are contrasted in Fig. 9. It is clear that after the operation time interval (time required for generating parameter estimates), the consequently tuned IRC-based scheme delivers performance almost matching the one delivered by the optimally tuned one.

It was also noted that after the first estimation, the closed-loop system presents very small oscillations and the estimator was unable to produce any further estimates.

***3) Case 3—Online Tuning of the IRC Scheme When Payload is Decreased (Resonance Frequency Increases):*** This last experiment aims to mimic the removal of the payload from a nanopositioner that is working with a control scheme designed to operate with the payload (appropriate resonance frequency). The same reasoning as in the previous case is applied, but in reverse. In this case, parameters of the $Y$-axis of the nanopositioner are first used to design the IRC-based control scheme by using (16), then this control scheme is applied to the $X$-axis and tracking performance is ascertained using the same 35-Hz triangular trajectory. The algebraic estimator is triggered to estimate the parameters of the $X$-axis and to redesign the parameters of the controller in order to improve its performance. The experimental results obtained are shown in Fig. 9. It is important to note that in this case, the algebraic estimator needs a longer time interval to produce the estimates of the parameters of the system than in the case of addition of payload. This is because a removal of the payload of the system leads to smaller residual

TABLE III
PERFORMANCE COMPARISON

| Case | $\omega_n$ error | $\sigma$ error | $\zeta$ error |
|---|---|---|---|
| Without previous knowledge | 4.63% | 7.8% | 174% |
| Increased payload | 1.45% | 5.22% | 180% |
| Decreased payload | 30.51% | 33.36% | 150% |

Quantifying controller estimator performance

| | IRC estimator-based tuned | | IRC incorrectly tuned | |
|---|---|---|---|---|
| Index | Payload↑ | Payload↓ | Payload↑ | Payload↓ |
| ISE: | 0.00009 | 0.00006 | 0.0016 | 0.00046 |
| IAE: | 0.0015 | 0.0012 | 0.0058 | 0.0034 |
| ITAE: | 0.00002 | 0.00001 | 0.00008 | 0.00005 |

vibrations in the tracking of reference signals due to increase in resonance frequency and the lower amplitude of the relevant harmonic component in the triangular trajectory that excites it.

***4) Performance of the Proposed Algorithm:*** The experimental results obtained in the three aforementioned cases, i.e., no previous knowledge of the system, addition of mass, and removal of mass are summarized in Table III. This table, on the one hand, quantifies the performance of the algebraic estimator, by presenting the errors in the estimates of the three parameters of the system, i.e., $\omega_n$, $\sigma$, and $\zeta$, and, on the other hand, compares the performance of the classical IRC scheme versus the proposed algorithm in the tracking of a triangular signal. In order to compare these two schemes, the classical measures of controlled system performance are utilized, i.e., integral squared error (ISE), integral absolute error (IAE) and integral time-weighted absolute error (ITAE). It is important to note that in this case, the goal was not to track the triangular signal without error, but to reproduce the tracking capabilities of the IRC scheme designed by considering a perfect knowledge of the parameters of the system, this is why the different error indexes are computed considering the difference with the signal produced by the IRC optimally tuned.

It can be seen from the data presented in Table III that the proposed control scheme produces very accurate estimates of the parameters of the system and therefore leads to a tuning of the IRC that is very closed to the case with complete knowledge of the parameters of the system, thus producing much better control performance when compared with the traditional IRC without automatic tuning.

## V. CONCLUSION

The algebraic framework for the full parametric identification of lightly damped second-order systems was expounded and further combined with a suitable reinitiation algorithm to enable the generation of accurate parameter estimates within one period of the resonance frequency. Simulations as well as experiments carried out on a nanopositioner validated the efficacy of the proposed technique. Closed-loop tracking results obtained via the proposed online estimation and consequent control scheme tuning were in good agreement with those obtained via an optimally tuned control scheme and clearly outperformed the static pretuned control scheme in presence of parametric variations. This was demonstrated by using the popular and simple IRC-based control scheme implemented on a serial-kinematic $XY$ nanopositioner forced to track typical triangular trajectories. Future research directions include increasing the number of system parameters that can be estimated, investigating methods to reduce estimation errors, and incorporating automatic optimal tuning of more evolved control schemes.

## REFERENCES


[1] E. Avci *et al.*, "High-speed automated manipulation of microobjects using a two-fingered microhand," *IEEE Trans. Ind. Electron.*, vol. 62, no. 2, pp. 1070–1079, Feb. 2015.

[2] T. Uchihashi, H. Watanabe, S. Fukuda, M. Shibata, and T. Ando, "Functional extension of high-speed AFM for wider biological applications," *Ultramicroscopy*, vol. 160, pp. 182–196, 2016.

[3] K. Yoshida, K. Tanaka, T. Tsujimura, and Y. Azuma, "Assisted focus adjustment for free space optics system coupling single-mode optical fibers," *IEEE Trans. Ind. Electron.*, vol. 60, no. 11, pp. 5306–5314, Nov. 2013.

[4] D. Min, M. A. Arbing, R. E. Jefferson, and J. U. Bowie, "A simple DNA handle attachment method for single molecule mechanical manipulation experiments," *Protein Sci.*, vol. 25, no. 8, pp. 1535–1544, 2016.

[5] C. Hyun, H. Kaur, T. Huang, and J. Li, "A tip-attached tuning fork sensor for the control of DNA translocation through a nanopore," *Rev. Sci. Instrum.*, vol. 88, no. 2, 2017, Art. no. 025001.

[6] A. Fleming, *Design, Modeling and Control of Nanopositioning Systems* Advances in Industrial Control. New York, NY, USA: Springer, 2014.

[7] S. O. R. Moheimani, "Invited review article: Accurate and fast nanopositioning with piezoelectric tube scanners: Emerging trends and future challenges," *Rev. Sci. Instrum.*, vol. 79, no. 7, 2008, Art. no. 071101.

[8] A. J. Fleming, S. S. Aphale, and S. O. R. Moheimani, "A new method for robust damping and tracking control of scanning probe microscope positioning stages," *IEEE Trans. Nanotechnol.*, vol. 9, no. 4, pp. 438–448, Jul. 2010.

[9] Z. Feng, J. Ling, M. Ming, and X. Xiao, "Data-driven feedforward decoupling filter design for parallel nanopositioning stages," in *Proc. Int. Conf. Intell. Robot. Appl.*, 2016, pp. 709–720.

[10] M. Mahmoodi, J. K. Mills, and B. Benhabib, "A modified integral resonant control scheme for vibration suppression of parallel kinematic mechanisms with flexible links," *Int. J. Mechatronics Automat.*, vol. 5, no. 1, pp. 44–57, 2015.

[11] A. Sebastian and S. Salapaka, "Design methodologies for robust nanopositioning," *IEEE Trans. Control Syst. Technol.*, vol. 13, no. 6, pp. 868–876, Nov. 2005.

[12] S. S. Aphale, A. Ferreira, and S. R. Moheimani, "A robust loop-shaping approach to fast and accurate nanopositioning," *Sens. Actuators A: Phys.*, vol. 204, pp. 88–96, 2013.

[13] S. K. Das, H. R. Pota, and I. R. Petersen, "Damping controller design for nanopositioners: A mixed passivity, negative-imaginary, and small-gain approach," *IEEE/ASME Trans. Mechatronics*, vol. 20, no. 1, pp. 416–426, Feb. 2015.

[14] S. K. Das, H. R. Pota, and I. R. Petersen, "Multivariable negative-imaginary controller design for damping and cross coupling reduction of nanopositioners: A reference model matching approach," *IEEE/ASME Trans. Mechatronics*, vol. 20, no. 6, pp. 3123–3134, Dec. 2015.

[15] S. K. Das, O. U. Rehman, H. R. Pota, and I. R. Petersen, "Minimax LQG controller design for nanopositioners," in *Proc. Eur. Control Conf.*, Jun. 2014, pp. 1933–1938.

[16] M. Fliess and H. Sira-Ramírez, "An algebraic framework for linear identification," *ESAIM: Control, Optim. Calculus Variation*, vol. 9, pp. 151–168, 2003.

[17] E. Pereira, J. R. Trapero, I. M. Díaz, and V. Feliu, "Algebraic identification of the first two natural frequencies of flexible-beam-like structures," *Mech. Syst. Signal Process.*, vol. 25, no. 7, pp. 2324–2335, 2011.

[18] E. Pereira, J. Trapero, I. Díaz, and V. Feliu, "Adaptive input shaping for manoeuvring flexible structures using an algebraic identification technique," *Automatica*, vol. 45, no. 4, pp. 1046–1051, 2009.

[19] J. C. Cambera, A. San-Millan, and V. Feliu-Batlle, "Payload mass identification of a single-link flexible arm moving under gravity: An algebraic identification approach," *Shock Vibration*, vol. 2015, pp. 1–13, 2015.

[20] Y. Tian, B. Shirinzadeh, and D. Zhang, "A flexure-based mechanism and control methodology for ultra-precision turning operation," *Precis. Eng.*, vol. 33, no. 2, pp. 160–166, 2009.
[21] M. Karimi-Ghartemani, H. Karimi, and M. R. Iravani, "A magnitude/phase-locked loop system based on estimation of frequency and in-phase/quadrature-phase amplitudes," *IEEE Trans. Ind. Electron.*, vol. 51, no. 2, pp. 511–517, Apr. 2004.
[22] M. Mojiri and A. R. Bakhshai, "An adaptive notch filter for frequency estimation of a periodic signal," *IEEE Trans. Autom. Control*, vol. 49, no. 2, pp. 314–318, Feb. 2004.
[23] M. Hou, "Amplitude and frequency estimator of a sinusoid," *IEEE Trans. Autom. Control*, vol. 50, no. 6, pp. 855–858, Jun. 2005.
[24] G. Fedele and A. Ferrise, "Non adaptive second-order generalized integrator for identification of a biased sinusoidal signal," *IEEE Trans. Autom. Control*, vol. 57, no. 7, pp. 1838–1842, Jul. 2012.
[25] G. Fedele and A. Ferrise, "A frequency-locked-loop filter for biased multi-sinusoidal estimation," *IEEE Trans. Signal Process.*, vol. 62, no. 5, pp. 1125–1134, Mar. 2014.
[26] M. R. Osborne and G. K. Smyth, "A modified prony algorithm for exponential function fitting," *SIAM J. Sci. Comput.*, vol. 16, no. 1, pp. 119–138, 1995.
[27] J. R. Trapero, H. Sira-Ramírez, and V. F. Batlle, "A fast on-line frequency estimator of lightly damped vibrations in flexible structures," *J. Sound Vib.*, vol. 307, no. 1, pp. 365–378, 2007.
[28] A. San-Millan and V. Feliu, "A fast online estimator of the two main vibration modes of flexible structures from biased and noisy measurements," *IEEE/ASME Trans. Mechatronics*, vol. 20, no. 1, pp. 93–104, Feb. 2015.
[29] J. Cortes-Romero, C. Garcia-Rodriguez, A. Luviano-Juarez, and H. Sira-Ramírez, "Algebraic parameter identification for induction motors," in *Proc. 37th Annu. Conf. IEEE Ind. Electron. Soc.*, Nov. 2011, pp. 1734–1740.
[30] R. Garrido and A. Concha, "An algebraic recursive method for parameter identification of a servo model," *IEEE/ASME Trans. Mechatronics*, vol. 18, no. 5, pp. 1572–1580, Oct. 2013.
[31] G. Mamani, J. Becedas, V. Feliu-Batlle, and H. Sira-Ramírez, "Open- and closed-loop algebraic identification method for adaptive control of DC motors," *Int. J. Adaptive Control Signal Process.*, vol. 23, no. 12, pp. 1097–1103, Mar. 2009.
[32] J. Mikusinski and T. Boehme, *Operational Calculus*, 2nd ed., vol. I. New York, NY, USA: Pergamon, 1987.
[33] S. E. R. L. Allison Jones, and Charles W. Champ, "The performance of exponentially weighted moving average charts with estimated parameters," *Technometrics*, vol. 43, no. 2, pp. 156–167, 2001.
[34] D. Russell, A. J. Fleming, and S. S. Aphale, "Simultaneous optimization of damping and tracking controller parameters via selective pole placement for enhanced positioning bandwidth of nanopositioners," *J. Dyn. Syst., Meas., Control*, vol. 137, no. 10, pp. 101004–101012, Jul. 2015.

**Andres San-Millan** received the M.Sc. (Hons.) and Ph.D. degrees in industrial engineering from the Universidad de Castilla-La Mancha, Ciudad Real, Spain, in 2011 and 2017.

He is currently a Postdoctoral Researcher at the Ecole Polytechnique Fédérale de Lausanne, Lausanne, Switzerland, where he has been engaged in the modeling and control of soft robots. His research interests include the active damping of vibrations in flexible structures and the dynamic control of flexible and soft robots.

**Sumeet S. Aphale** (M'09–SM'18) received the bachelor's degree from the University of Pune, Pune, India, in 1999, and the M.S. and Ph.D. degrees from the University of Wyoming, Laramie, WY, USA, in 2003 and 2005, respectively, all in electrical engineering.

He was a member of the Australian Research Council's Centre of Excellence for Complex Dynamic Systems and Control, The University of Newcastle, Callaghan, Australia, from 2005 to 2008 and was also a Research Fellow with the Centre for Applied Dynamics Research, University of Aberdeen from 2008 to 2009. He is a Senior Lecturer with the University of Aberdeen, Aberdeen, U.K., focusing his efforts on vibration control, nanopositioning, and control of nonlinear systems.

**Vicente Feliu** (M'88–SM'08) received the M.Sc. (Hons.) degree in industrial engineering and the Ph.D. degree in automatic control from the Polytechnic University of Madrid, Madrid, Spain, in 1979 and 1982, respectively.

From 1980 to 1994, he was in the Electrical Engineering Department, Universidad Nacional de Educacion a Distancia, Madrid, Spain, where he was a Full Professor in 1990, and the Head of the Department from 1991 to 1994. From 1994 to 2008, he has been the Dean of the School of Industrial Engineering, Universidad de Castilla-La Mancha, Ciudad Real, Spain. His research interests include multivariable and digital control systems, fractional dynamics and control, kinematic and dynamic control of rigid and flexible robots, and mechatronics.